ACS APPLIED MATERIALS & INTERFACES

Research Article

www.acsami.org

Light-Assisted Anodized TiO_2 Nanotube Arrays

York R. Smith,[†] Biplab Sarma,[†] Swomitra K. Mohanty,[‡] and Mano Misra*[,†,‡]

[†]Metallurgical Engineering Department and [‡]Chemical Engineering Department, University of Utah, Salt Lake City, Utah 84112, United States

Supporting Information

ABSTRACT: Self-assembled arrays of titania nanotubes are synthesized via electrochemical anodization of Ti foils under the presence of UV−vis irradiation. Compared to control samples (anodized without light), the light-assisted anodized samples exhibit larger diameters as well as thicker nanotube walls, whereas the length of the nanotubes remains the same under otherwise similar synthesis conditions. Enhanced photoelectrochemical performance with light-assisted anodized samples under simulated AM 1.5 irradiation is observed by an increase in photocurrent density of 45−73% at 1.23 V (RHE). The enhanced photoelectrochemical performance is correlated to improved charge separation analyzed by Mott−Schottky. A mechanism on the photoeffect during anodization is presented. The morphology and improved properties obtained from the synthesis methodology may also find application in other fields such as sensing and catalysis

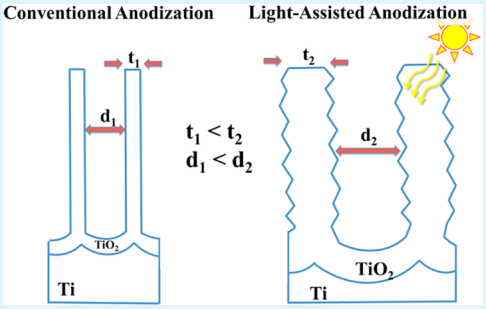

KEYWORDS: *TiO_2 nanotube arrays, anodization, light assisted anodization, photoelectrochemical hydrogen, electrochemical impedance spectroscopy, Mott−Schottky*

1. INTRODUCTION

Zwilling and co-workers first reported the synthesis of self-organized nanotube arrays on titanium and titanium alloys achieved through electrochemical anodization in the presence of fluoride ions.[1,2] Subsequently, several approaches have been made to improve the geometry and developing an understanding of the nanotube formation mechanism.[3−7] The improvements in the synthesis of titania nanotube arrays (TiO_2−NTA) over the past decade have demonstrated promising applications in many areas such as solar-based applications (i.e., photocatalysis,[8,9] photoelectrochemical,[10,11] and photovoltaic cells[12,13]), electrochromic devices,[14,15] sensors,[16,17] hydrogen storage,[18,19] and biomedical implants,[18,19] among others. The widespread use of this material can be ascribed to the fact that the synthesis method allows for easy control of tubular geometry at the nanoscale and the synthesis method is a scalable electrochemical process. Moreover, the growth of the nanotubes is not limited to planar substrates. Concave[20] as well as nonplanar or curved substrates such as wires[21,22] or mesh[23−25] have also been used for nanotube growth. We have also recently demonstrated site-specific and patterned growth of TiO_2−NTA on thin sputtered films of Ti on Si wafer.[26,27] For further details on the formation mechanism and applications of titania nanotube arrays, readers are directed to the recent review works of Schmuki[28] and Misra.[29]

Despite the widespread applications of TiO_2−NTA, the majority of studies on TiO_2−NTA remain in the realm of solar-based applications because of enhanced charge transport properties from the 1D architecture. As a result, several studies have been conducted on different methods to improve the photoactivity of TiO_2−NTA through band gap engineering (doping),[30−32] functionalizing/sensitizing with cocatalysts/heterostructure,[8,33−35] plasma surface treatments,[36] or used as a precursor to synthesize other photoactive materials such as bismuth titanate.[37] In many of these methods, treatment/functionalization of the TiO_2−NTA are performed ex situ, or post anodization. Modification of the TiO_2−NTA in situ during the anodization process to improve the phototelectrochemical (PEC) performance is a more desirable approach from engineering and manufacturing standpoint. In our previous investigations, we have demonstrated that carbon can be doped into the TiO_2−NTA during anodization by use of an organic electrolyte.[10] More recently, tungstate species can be coupled with TiO_2−NTA during anodization by use of tungstate anions in the electrolyte for improved PEC performance.[38] Sonoelectrochemical anodization has been a method we have employed to improve nanotube formation as well as enhance PEC activity.[41,42]

The use of other external stimuli during the anodization process for titania nanotube synthesis such as light, for example, has yet to be fully examined. Harris and Wilson[39] examined the photoelectrochemical stability of rutile titania in 1 N H_2SO_4. They observed that the capacitance of the electrode/electrolyte interface, quantum efficiency (PEC), and surface morphologies are all affected by exposure to light under an applied bias. Subsequent studies have utilized photoelectrochemical etching (PEC-E) to fabricate microstructures on the surface crystalline semiconductors.[44−47] For example, a honeycomb-type surface morphology is obtained through PEC-E of crystalline rutile

Received: August 1, 2012
Accepted: October 19, 2012
Published: October 19, 2012

titania in H_2SO_4.[40] This type of morphology is a result of preferential etching of the (001) crystal face. Improvement in PEC performance of single crystal rutile n-TiO_2 electrodes from PEC-E has been reported.[41] The improved PEC and photoluminescence in their study was concluded to be a result of increased surface area due to micropore formation and a more activated surface for water oxidation reaction due to PEC-E treatment. These studies have focused on preformed crystalline rutile titania surfaces using H_2SO_4 as the etching agent. PEC-E has also been extended to Si substrates for the fabrication of porous Si by using n-type Si where photoinduced holes are required for etching reaction[42] and generally HF is used as the etching agent.

Here we report the synthesis of TiO_2–NTA under UV–vis irradiation and its application in photoelectrochemical hydrogen generation. Anodization under irradiation results in larger diameter nanotubes with thicker walls and rougher, rippled sidewalls while the nanotube length remains the same compared to nanotubes prepared without UV–vis irradiation. The thicker, rippled walled nanotubes allows for greater band bending and reducing charge recombination resulting in enhanced PEC performance. The nanotube morphology thus obtained from light-assisted anodization may also provide more surface area for anchoring of dye molecules in dye sensitized or other sensitizers such as quantum dots or nanocrystals for improved cell performance, sensors, or capacitance applications.

2. EXPERIMENTAL SECTION

2.1. Light-Assisted Anodization. A depiction of the experimental setup for anodization under irradiation is shown in Scheme 1. Samples were prepared without irradiation (referred to as T-NTA), 1 h irradiation (referred to as T-NTA-60), and 0.5 h irradiation for the latter half of anodization time (referred to as T-NTA-30) under the experimental setup (Scheme 1). UV–vis irradiation of the Ti substrates during anodization was supplied by a medium pressure mercury immersion-type lamp (Ace glass, 7825–34) with a quartz water jacket. The bath temperature was maintained at 30 ± 5 °C throughout the experiment. The light intensity during anodization was held constant and measured to be 72.4 mW/cm^2 (Newport 70260, radiant power meter). Titania nanotube synthesis procedure was carried out similar to a previous report.[43] In summary, Ti foils (1.5 × 2 cm, ESPI Metals, G1 grade) were degreased under ultrasonication for 15 min in a 50/50 vol% acetone/isopropanol solution. After drying in air, one side of the Ti foil was masked with Kapton tape for TiO_2–NTA growth to occur on one side of the substrate. Anodization was carried out at 60 V for a total of 1 h in a fluorinated solution of ethylene glycol (0.25 wt % NH_4F, 10 wt % DI H_2O) under mechanical stirring with a Pt gauze (52 mesh) cathode. Post-anodization, the samples were washed thoroughly with isopropanol and DI water followed by drying at 110 °C in air for a few hours. Crystallization of the amorphous TiO_2–NTA was executed at 500 °C for 2 h under N_2/H_2 (5% H_2, N_2 balance) atmosphere with a heating rate of 1.5 °C/min.

Scheme 1. Depiction of the Top View of the Experimental Setup Used for Anodization in the Presences of UV–Vis Irradiation[a]

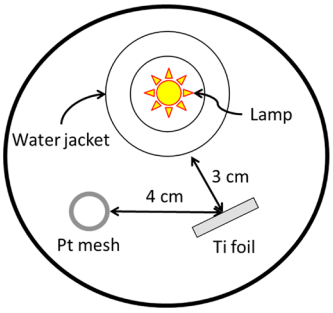

[a]Light is supplied via immersion lamp and the temperature is maintained by water circulation jacket.

2.2. Characterization. Scanning electron micrographs (SEM) were collected using a field-emission Hitachi S-4800. X-ray diffraction (XRD) was performed system with CuKα radiation (λ = 1.54 Å) between the ranges of $2\theta^o$ = 20–60 at a rate of 0.025 °/s. X-ray photoelectron spectroscopy (XPS) was collected using the monochromatic AlKα source (PE = 1600 eV) on a Kratos Axis Ultra DLD instrument, with a 300 - 700 μm spot size. Dwell time was 200 ms with three sweeps and a step size of 1 eV (0.1 eV for regional scans). UV–vis diffuse reflectance was performed on a UV-3600 Shimadzu UV–vis-NIR spectrophotometer.

2.3. Photoelectrochemical Studies. Photoelectrochemical (PEC) tests were conducted in a custom-built cell with a quartz window. The photoanodes were irradiated with a 300 W solar simulator (6991, Newport-Oriel) with Pt gauze as the cathode and Ag/AgCl (3 M KCl) as the reference electrode. All PEC experiments were conducted under AM 1.5 irradiation by use of an optical filter. A 1 M KOH (pH = 13.8) electrolyte was used while a computer-controlled potentiostat (Princeton Applied Research, Parstat 4000) was used to collect potentiodynamic and potentiostatic plots. For potentiodyamic studies, the photoanodes were polarized under irradiation anodically from open-circuit potential (OCP) at a scan rate of 10 mV/s. Potentiodynamic experiments were collected at 0.5 V (vs Ag/AgCl) while cycled through on/off illumination. Mott–Schottky (M–S) experiments were conducted under irradiation using a Gamry Reference 600 potentiostat at 1 kHz within the potential window of 1 to −1 V (vs Ag/AgCl) with an AC imposed voltage of 10 mV.

3. RESULTS

3.1. Anodic Polarization. Figure 1 shows the anodic polarization behavior of a Ti foil in the anodization electrolyte with and without illumination accompanied with representative SEM images. The polarization was carried out from the open-circuit potential (OCP) to 5 V (vs Ag/AgCl) at 1 mV/s. Under illumination, the critical current density for passivation occurs at a higher potential. The saturation current density without light is 0.52 mA/cm^2, whereas polarization with light gives a saturation current density of 1.47 mA/cm^2. In general, the anodic current has two components; namely (1) current due to oxide formation and (2) current due to oxidative dissolution.[44] When examining the surface after polarization under both conditions, the initial formation of a nanotube structure can be observed (inset images of Figure 1). In the absence of light, the pores/nanotubes have an average outer diameter of 20 nm. Upon polarization under light, the pores/nanotubes form larger diameter (22 nm).

3.2. Anodization. The current–time plots obtained from anodization under various conditions for one hour are shown in Figure 2. The anodization profile without illumination (Figure 2A-a) shows a typical current–time profile for nanotube formation,[3] which occurs in three stages: (i) initial decrease in current due to oxide barrier formation, (ii) slight increase in current due to pitting/nanotube formation from fluoride ions, and (iii) saturation current due to stead-state nanotube growth. The final current density for T-NTA was 1.03 mA/cm^2. Figure 2A-b shows the anodization profile for T-NTA-30, in which the first 1800 s of anodization is without irradiation and hence the similar anodization profile for T-NTA. Anodization under irradiation for the entire anodization duration (Figure 2A-c, sample T-NTA-60) shows greater pitting/nanotube formation,

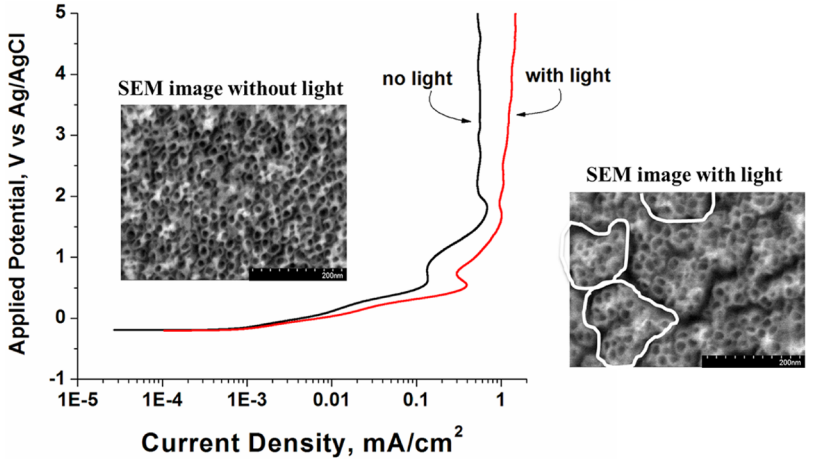

Figure 1. Anodic polarization of a Ti foil with and without UV–vis irradiation. The inset images are representative SEM images of the Ti surface after polarization with and without irradiation. Bundles of the nanotubes formed with light assisted anodization are highlighted. Both anodes were polarized at 1 mV/s from open circuit potential to 5 V in ethylene glycol +10 wt % H_2O + 0.5 wt % NH_4F.

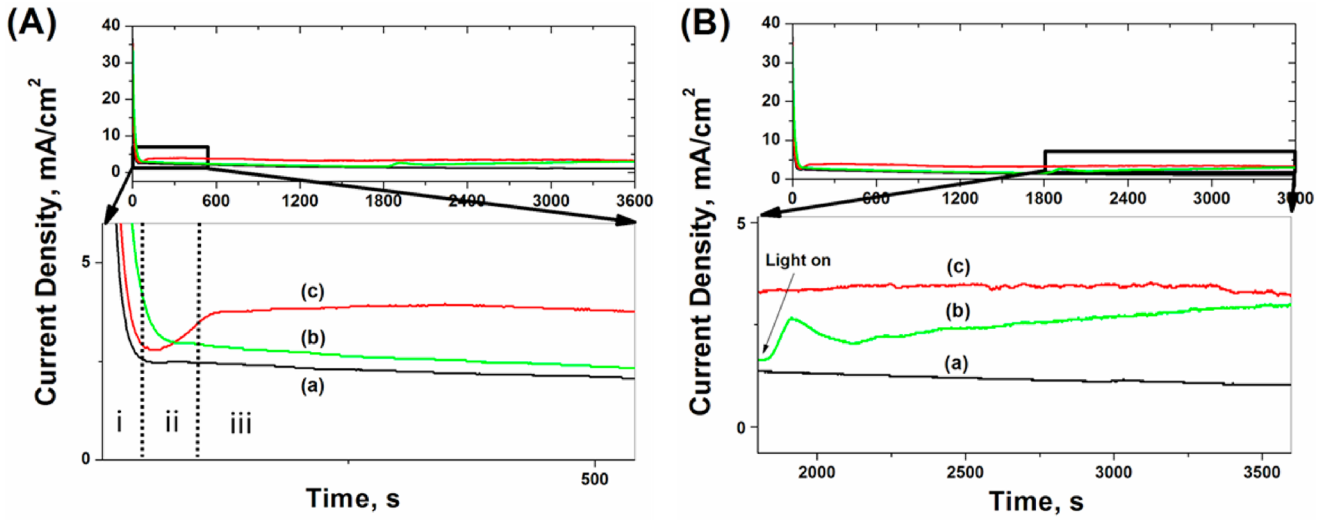

Figure 2. Transient current density of (a) T-NTA, (b) T-NTA-30, and (c) T-NTA-60 during anodization during the (A) initial stage of anodization showing nanotube growth in three stages: (i) initial decrease in current due to oxide barrier formation, (ii) slight increase in current due to pitting/nanotube formation from fluoride ions, and (iii) saturation current due to nanotube growth. (B) The remaining 1800 s of anodization where sample T-NTA-30 was exposed to irradiation for the final 1800 s. Anodization was carried out for 3600 s in ethylene glycol +10 wt % H_2O + 0.5 wt % NH_4F at 60 V.

which is evident from the more pronounced dip in current density followed by increased saturation current density (3.20 mA/cm^2). For the T-NTA-30 sample, the lamp was turned on at the 0.5 h mark. Before illumination the T-NTA-30 had an anodization current density of 1.63 mA/cm^2 (1.36 mA/cm^2 for T-NTA) and when irradiated, the current profile shows sudden increase in current density followed by a gradual decrease in current density. Subsequently, the current density gradually increases under illumination reaching a steady increase in current density of 3.00 mA/cm^2 at the end of the anodization time. It is interesting to note, the increase in current density under illumination from the polarization plots and anodization current–time plots, all show approximately a three-time increase in current density when the anode is under illumination during anodization.

3.3. Surface Characterization. Scanning electron micrographs were collected to examine the surface morphology of the titania nanotubes when synthesized under light stimuli (Figure 3). A summary of the nanotube dimensions (i.e., outer diameter, wall thickness, and nanotube length) is given in Table 1. From the data in Table 1, and the SEM images in Figure 3, it is observed that light-assisted anodization results in thicker walls with more pronounced rippled sidewalls. It is also observed that the length of the nanotubes remains essentially the same regardless of light stimuli during anodization. Consistency in tube length suggests that the increased anodization current due to light stimuli during anodization contributes to wall growth and forming larger diameter nanotubes over increasing the length of the nanotube. A discussion on a possible mechanism for the influence of light during anodization on nanotube morphology is given in Section 4.

3.4. X-ray- Diffraction & Photoelectron Spectroscopy. X-ray diffraction (XRD) was carried out on annealed samples to determine the crystalline phases of the nanotubes. The XRD patterns (see the Supporting Information, Figure S2) have been indexed to standard JCPDS cards. All samples show anatase phase titania (labeled 'A', JCPDS #: 21–1272) indicated by

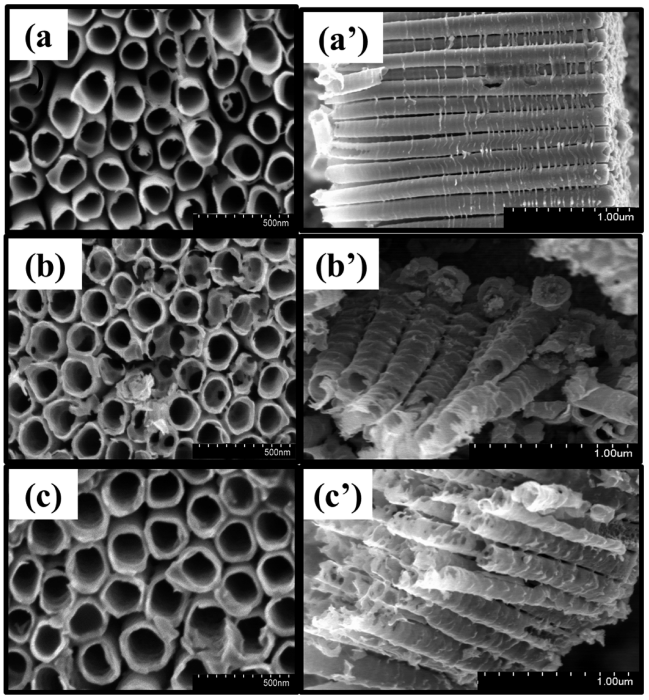

Figure 3. SEM images of the (a) top and (a′) sidewall of T-NTA, (b, b′) T-NTA-30, and (c, c′) T-NTA-60.

Table 1. Summary of Nanotube Dimensions Obtained from SEM Analysis

sample	outer diameter (nm)	wall thickness (nm)	nanotube length (μm)
T-NTA	159 ± 8	14 ± 0.7	1.9 ± 0.1
T-NTA-30	178 ± 9	19 ± 1.0	1.8 ± 0.1
T-NTA-60	200 ± 10	28 ± 1.4	1.9 ± 0.1

peaks at $2\theta^{o}$ = 25.5, 48.2, 54.0, and 55.2 as well as a shoulder at $2\theta^{o}$ = 38.0, which is overlapping with a diffraction peak of Ti ($2\theta^{o}$ = 38.6). Other Ti peaks (labeled 'T', JCPDS #: 44−1294) are observed at $2\theta^{o}$ = 40.4 and 53.2. A decrease in intensity of the anatase peaks is noted for samples anodized under light conditions. More detailed studies are required to understand this observation and are a part of future work.

Anodization in an organic electrolyte with subsequent annealing in a reducing atmosphere results in carbon doping of the nanotubes.[10] In the absence of oxygen during the annealing process the organics are not burned off, but decompose to generate free carbon resulting in high residual carbon content within the TiO_2−NTA. During the annealing process, the TiO_2−NTA crystallizes and the carbon becomes doped simultaneously. To further examine if the amount of carbon doping increases when the nanotubes are synthesized under irradiation, we carried out high-resolution X-ray photoelectron spectroscopy (XPS). All samples were exposed to Ar^+ for 60 s to remove ∼10 nm of the surface layer to reflect the bulk composition. Figure 4 shows the regional scan for the C s1 spectra. It is evident that all three samples exhibit four C s1 peaks. For example, T-NTA sample has peaks at 288.2, 282.1, 286.6, and 284.8 eV. The C s1 peaks around 284.8 eV can be assigned to adventitious carbon (C−C), which is present in all samples and is unavoidable contamination. The peaks around 282.1 eV are close to the C s1 peak for Ti−C[45] which can be due to carbon substitution of oxygen atoms within the

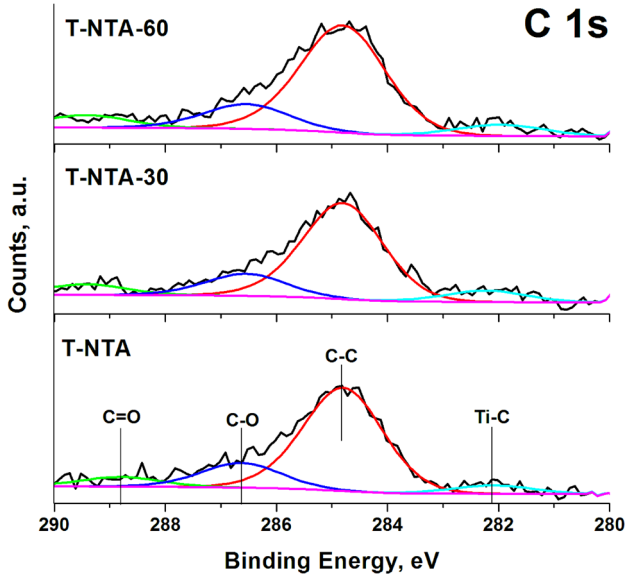

Figure 4. Regional X-ray photoelectron spectra for C s1 of the various samples. Curves labeled C−C are due to adventitious carbon, whereas curves labeled Ti−C, C−O, and C═O are due to doped carbon and Ti-carbonate species.

titania lattice forming O−Ti−C. Integration of these peaks gives rise to the amount of doped carbon in each sample, which is 5.74, 8.35, and 7.28% for samples T-NTA, T-NTA-30, and T-NTA-60, respectively. Light assisted anodization results in approximately 27−45% more carbon doping, but longer anodization under irradiation (T-NTA-60) dose not lead to increased carbon loading. Despite recently improved models describing the formation of porous anodic films, current models do not account for point defects or incorporation of electrolyte species as to date.[7] There may be some leaching effect or saturation of carbonaceous species due to the synthesis method. Further studies are underway to understand these observations. The peaks around 286.6 eV can be assigned to Ti−C−O bonds, forming carbonate species,[46] whereas the peaks around 288.8−289.4 eV can be ascribed to C═O carbonate species.[47]

Annealing in a reducing atmosphere can also lead to the formation of substoichiometric TiO_2 oxidation states. These oxygen vacancies can assist with enhancing photocurrent by improving charge transport.[48,49] The Ti 2p spectra of the samples are given in the Supporting Information (Figure S3). From the spectra, all the samples show $2p_{1/2}$ and $2p_{3/2}$ Ti^{4+} binding energies of 464.7 and 459.1 eV, respectively. Substoichiometric oxidation states are evident from the shoulders at ∼457.3 and ∼455.5 eV for Ti^{3+} and Ti^{2+}, respectively.

3.5. UV−Vis Diffuse−Reflectance. The Diffuse−reflectance absorbance spectra are shown in Figure 5. The nanotubes contain mainly anatase phase titania (Figure 4) which has a band gap of 3.2 eV. T-NTA sample has an indirect band gap of 3.2 eV with a long-tail absorption from 370 to 800 nm. Upon interstitial substitution of carbon in the titania lattice, carbonate species form, which results in a long-tail absorption within the visible region.[50] Ethylene glycol is oxidized during the anodization process to form carbonate species, which are adsorbed by the outer layer of the nanotube walls. When subject to thermal treatment in hydrogen atmosphere, the adsorbed carbonate species possibly reduce to carbon species and diffuse into the nanotube walls. A slight red shift in the

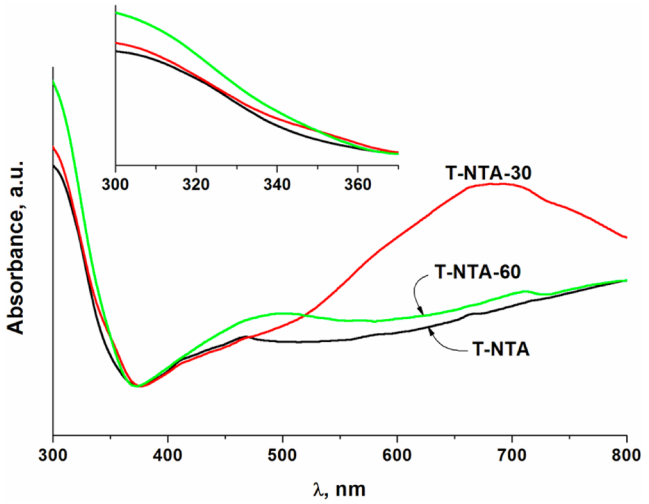

Figure 5. Diffuse−reflectance absorbance spectra of the samples. Inset shows an expanded region between 300 and 370 nm. Light-assisted anodized samples show increased visible-light absorbance.

onset absorbance edge is observed from T-NTA-30 and T-NTA-60 where the indirect band gap is estimated to be 3.1 and 2.9 eV, respectively. The inset of Figure 6 shows highlights absorbance spectra from 300 to 370 nm, showing a shoulder at 360 nm for T-NTA-30 and T-NTA-60. The light assisted anodized samples show a stronger absorbance tail within the visible light spectrum with enhanced absorbance between 460 and 800 nm for T-NTA-30, specifically. A higher loading of carbon doping (XPS data) may account for the increased visible light absorbance of T-NTA-30 sample. However, the contribution of substoichiometric titania to the increased visible light absorbance should not be discounted. Self-doping (oxygen vacancies) as a result of thermal treatment in a reducing atmosphere can lead to long-tail visible light absorbance due to narrow impurities in the conduction band.[51] The band gap states and increasing visible-light absorbance could be attributed to oxygen vacancies introduced by annealing in hydrogen and/or a result of carbonaceous species in the titania lattice substituting with the oxygen sublattice.[11,49]

3.6. Photoelectrochemical Studies. Figure 6 shows the potentiodynamic and potentiostatic plots and conversion efficiency of solar energy to chemical energy plots for the various samples irradiated by AM 1.5 simulated solar irradiation. The applied potential is reported against reversible hydrogen electrode (RHE), which is given by the relationship

$$E_{RHE} = E_{Ag/AgCl} + 0.059pH + 0.197V \quad (1)$$

A summary of the photoelectrochemical data obtained from these plots (i.e., open circuit potential (OCP), photocurrent density at 1.23 V_{RHE}) is given in Table 2. The light-assisted anodized samples show a 45−73% increase in photocurrent density, whereas all samples have similar OCP values (within 30 mV). Monitoring the photocurrent during discontinuous illumination can reveal information about the stability of the photoanodes.[52] On/off illumination of the photoanodes (Figure 6b) shows an instantaneous drop in photocurrent and quick recovery to the original photocurrent density through multiple on/off cycles. The dark photocurrent density for all the samples was recorded in the range of 20−60 $\mu A/cm^2$ at a bias of 1.5 V vs RHE (0.5 V vs Ag/AgCl), showing that the photocurrent generated is due to photoinduced charges from the titania samples.

Table 2. Summary of Photoelectrochemical Performance of the Anodes Obtained from Figure 7

sample	OCP, V (RHE)	J, mA/cm^2 (1.23 V, RHE)
T-NTA	0.178	0.561
T-NTA-30	0.180	0.811
T-NTA-60	0.150	0.973

The enhancement of PEC performance of the light assisted anodized samples can be explained by the results of Mott−Schottky plots (Figure 7) obtained through potentiodynamic electrochemical impedance spectroscopy under irradiation.

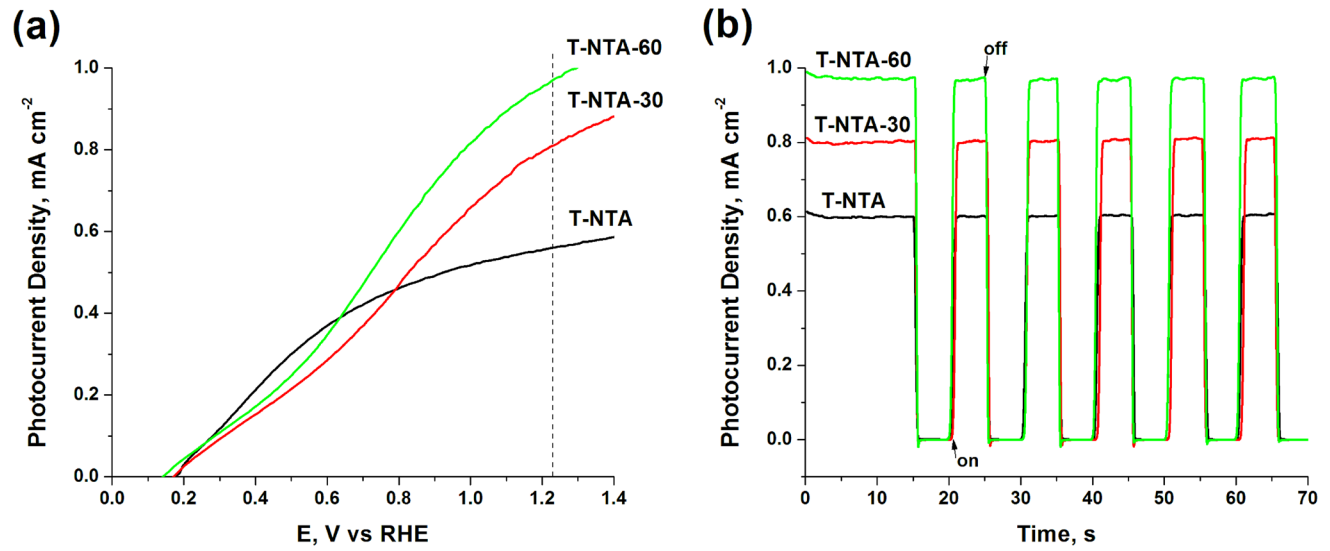

Figure 6. (a) Potentiodynamic plots, (b) potentiostatic plots at 1.5 V_{RHE} (0.5 V vs Ag/AgCl) cycled through on/off irradiation. The photoactivity was examined under AM 1.5 irradiation (87 mW/cm^2) in 1 M KOH electrolyte with a Pt mesh and Ag/AgCl serving as the counter and reference electrodes, respectively. Light assisted anodized samples show a 45−73% increase in photocurrent density.

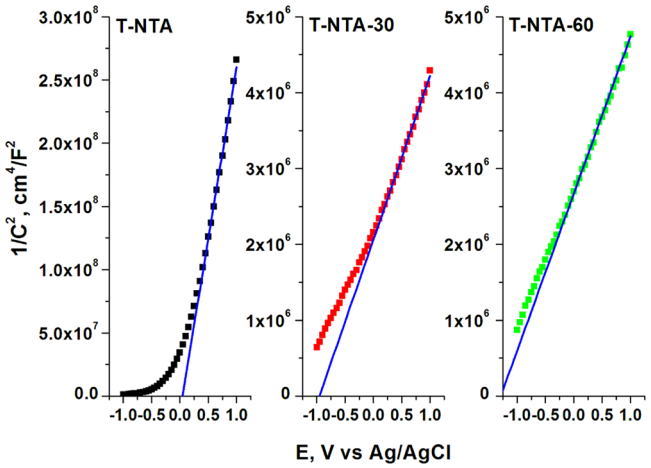

Figure 7. Mott–Schottky plots of the samples under AM 1.5 irradiation at a frequency of 1 kHz with an AC imposed bias of 10 mV in 1 M KOH electrolyte.

Electrochemical impedance spectroscopy (EIS) us a powerful tool for studying the interfacial properties between electrodes and solutions.[53] On the basis of well-documented theory of semiconductor/electrolyte interfacial capacitance, the electronic properties in terms of charge carrier density (N_A) and flat-band potential (E_{FB}) can be obtained from the Mott–Schottky equation:[54]

$$\frac{1}{C^2} = \frac{2}{\epsilon\epsilon_0 N_A}\left(-\Delta\phi - \frac{k_B T}{e}\right) \quad (2)$$

$$-\Delta\phi = E - E_{FB} \quad (3)$$

where, C is the capacitance, e is the elementary electronic charge, ϵ_0 is the permittivity in vacuum, ϵ is the dielectric constant, k_B is the Boltzmann constant, T is the temperature, and E is the applied bias. From the slope (m) of $1/C^2$ vs E plots in Figure 7, N_A can be determined by,

$$N_A = \frac{2}{\epsilon\epsilon_0 m} \quad (4)$$

where the intercept of the line yields E_{FB}. The linear portion of the $1/C^2$ vs E plots are fit within the potential domain in which the samples behave as capacitors. A summary of N_A and E_{FB} values is given in Table 3. A net shift of −0.99 to −1.23 V in E_{FB} in conduction band position for T-NTA-30 and T-NTA-60, respectively, is observed. Similar E_{FB} values were obtained within the frequency range of 1–5 kHz. Also, a two-order magnitude increase in charge carrier density (N_A) for light assisted anodization samples over T-NTA is noted. The large negative shift in E_{FB} for T-NTA-30 and T-NTA-60 indicates that greater band bending takes place with light assisted anodized samples under irradiation compared to T-NTA, which facilitates improved photoeffect with respect to electrolyte reorganization energy.[55] The increased N_A values for the light assisted anodized samples are due to effective separation of photogenerated electron and holes at the surface compared to that of T-NTA. A reduction in recombination of electron/hole pairs increases the lifetime of the minority charge carrier (holes) and in turn increases N_A. If it is assumed that band bending takes place across the wall thickness of the nanotubes, and not along the length of the nanotubes, greater band bending would occur within the thicker walled nanotubes, i.e., a larger depletion zone results in the formation of a localized electric field and subsequent increased lifetime of photoinduced charges. The electric field across the space charge layer drives photogenerated holes toward the solid–liquid interface and electrons toward the interior of the electrode and subsequently to the external circuit. Although it may be possible that the potential drop across the wall thickness is not large enough to separate photoinduced charges, it should be noted that the half-value of the wall thickness (Table 1) is less than the minority carrier diffusion length (20–30 nm for anatase TiO_2).[56] As a result, the holes can diffuse to the surface more readily. It has been shown that minority carriers generated within a distance from the surface comparable to the sum of the depletion layer width and the diffusion length escape recombination and reach the electrolyte.[57]

Table 3. Summary of Charge Carrier Density (N_A) and Apparent Flat-Band Potential (E_{FB}) Obtained from Mott–Schottky Analysis

sample	E_{FB} (V)[a]	N_A (cm^{-3})
T-NTA	0.042	1.08×10^{22}
T-NTA-30	−0.95	1.36×10^{24}
T-NTA-60	−1.29	1.45×10^{24}

[a]vs Ag/AgCl.

4. DISCUSSION

The use of light stimuli during the anodization process of titania nanotube synthesis demonstrates having a strong influence on surface morphology as well as photoelectrochemical performance. This section will discuss a possible mechanism for the observed nanotube morphology as a result of light assisted anodization.

The generalized mechanism for nanotube formation[28] still takes place; however, the change in nanotube morphology (i.e., diameter and wall thickness) under light anodized conditions can be attributed to the photoinduced holes. As-formed TiO_2–NTAs are not crystalline but amorphous in phase. Although amorphous in structure, the TiO_2–NTA can generate photoinduced charges.[48] Conduction band electrons and valence band holes are generated when the titania surface is illuminated with energy greater than the band gap ($E_g < h\nu$, eq 5). Due to the strong applied field, recombination of the electrons and holes (eq 6) is reduced and the majority of the electrons are driven to the external circuit by the strong electric field, hence the increase in current density observed during anodic polarization and during anodization (Figures 1-2). The strong anodic electric field aids in migrating bulk photoinduced holes to the surface of the titania. At the surface, the photoinduced holes react with water to form hydroxyl radials (eq 7). Hydroxyl radicals are highly reactive, nonselective oxidizing species. It is envisioned that the hydroxyl radicals aid in forming oxygenated species in solution, which serve as an oxygen source for oxide formation. These reactions may attribute to the thicker walled nanotubes anodized under illumination.

$$TiO_2 + h\nu \rightarrow TiO_2(e^- + h^+) \quad (5)$$

$$TiO_2(e^- + h^+) \rightarrow TiO_2 + \Delta \quad (6)$$

$$TiO_2(h^+) + H_2O \rightarrow TiO_2 + H^+ + OH^* \quad (7)$$

The increased wall thickness may be due to the hydroxyl radicals formed near the nanotube surface; however, it does not explain why anodization under light forms larger diameter nanotubes. It is possible that the holes help increase the migration Ti^{4+} ions to the surface due to Coulombic repulsive forces. It has been shown for the PEC-E of Si that electric field focusing effects can lead to the preferential transport of holes to the bottom of the pores.[42] Once the Ti^{4+} ions have migrated through the oxide, they are ejected at the oxide-electrolyte interface to form water-soluble fluoride species (eq 8).[28] The formation of $[TiF_6]^{2-}$ and the chemical attack of the TiO_2 via fluoride etching (eq 9) leads to the formation of pores.[58] By increasing the ejection of cations by hole migration to the surface and retarding the chemical etch rate, larger pores with a thicker oxide layer will be obtained. The base of the nanotubes (see the Supporting Information, Figure S1) are not only larger for the light anodized samples, but also exhibit interconnected interstitial voids between the bases and greater oxide formation in comparison. Generally, higher anodization current density correlates to increased oxide formation of valve metals,[59] which is evident from Figures 1 and 2.

$$Ti^{4+} + 6F^- \rightarrow [TiF_6]^{2-} \quad (8)$$

$$TiO_2 + 6HF \rightarrow [TiF_6]^{2-} + 2H_2O + 2H^+ \quad (9)$$

These claims are also supported by the increased rippled sidewall morphology of the light assisted anodized samples. The use of an organic electrolyte with a small amount of water (1 wt.%) results in smooth nanotube sidewalls, while controlled additions of water (1−10 wt %) to an organic electrolyte can be used to create defined sidewall modifications, i.e., sidewall ripples.[60] Similar morphologies can also be obtained by alternating the anodization voltage.[61] In both cases, either increasing the electrolyte water content or alternating the anodization potential results in oscillation of current density during anodization. The oscillation in current represents a fluctuation in the diffusion of participating species and results in rippled sidewall morphology. The more rippled sidewalls of the light-assisted anodized samples could be due to the photo-induced holes affecting the diffusion of cation species during anodization.

5. CONCLUSION

In summary, we have prepared TiO_2 nanotube arrays through anodization in the presence of UV−vis irradiation in a fluorinated organic electrolyte. Depending upon the exposure time to external light stimuli during anodization, larger inner diameter (140−144 nm) and thicker walled nanotubes (19−28 nm) are obtained with the same nanotube length. The larger nanotube dimensions of the nanotubes synthesized via light assisted anodization can be attributed to a higher concentration of H^+ at the base of the nanotubes during anodization due to photooxidation of water by the nanotubes. The photo-electrochemical activities of the light assisted anodized nanotubes are greater compared to nanotubes prepared using standard methods under simulated AM 1.5 irradiation. The photoelectrochemical performance of the titania nanotubes has been correlated to enhanced charge transport properties through Mott−Schottky analysis. Due to the morphology and enhanced optical and electronic properties, the application of the light assisted anodized titania nanotubes can be extended to other solar applications such as sensitized solar cells, as well as other applications such as sensors, Li-ion battery, and catalysis.

■ ASSOCIATED CONTENT

Supporting Information

SEM images of the base of the nanotubes, XRD, and Ti 2p XPS spectra. This material is available free of charge via the Internet at http://pubs.acs.org/

■ AUTHOR INFORMATION

Corresponding Author

*E-mail: mano.misra@utah.edu.

Notes

The authors declare no competing financial interest.

■ ACKNOWLEDGMENTS

The U.S. Department of Energy (DE-FC-36-06GO86066) supported the work presented here. The authors also thank Dr. Brian Van Devener for the XPS data and analysis.

■ REFERENCES

(1) Zwilling, V.; Aucouturier, M.; Darque-Ceretti, E. *Electrochim. Acta* **1999**, *45*, 921−929.
(2) Zwilling, V.; Darque-Ceretti, E.; Boutry-Forveille, A.; David, D.; Perrin, M. Y.; Ancouturier, M. *Surf. Interface Anal.* **1999**, *27*, 629−637.
(3) Raja, K. S.; Misra, M.; Paramguru, K. *Electrochim. Acta* **2005**, *51*, 154−165.
(4) Macak, J. M.; Sirotna, K.; Schmuki, P. *Electrochim. Acta* **2005**, *50*, 3679−3684.
(5) Macak, J. M.; Tsuchiya, H.; Taveira, L.; Aldabergerova, S.; Schmuki, P. *Angew. Chem., Int. Ed.* **2005**, *44*, 7463−7465.
(6) Raja, K. S.; Gandhi, T.; Misra, M. *Electrochem. Commun.* **2007**, *9*, 1069−1076.
(7) Hebert, K. R.; Albu, S. P.; Paramasivam, I.; Schmuki, P. *Nat. Mater.* **2012**, *11*, 162−166.
(8) Mohapatra, S. K.; Kondamudi, N.; Banerjee, S.; Misra, M. *Langmuir* **2008**, *24*, 11276.
(9) Smith, Y. R.; Kar, A.; Subramanian, V. R. *Ind. Eng. Chem. Res.* **2009**, *48*, 10268−10276.
(10) Mohapatra, S. K.; Misra, M.; Mahajan, V. K.; Raja, K. S. *J. Phys. Chem. C* **2007**, *111*, 8677−8685.
(11) Liu, Z.; Pesic, B.; Raja, K. S.; Rangaraju, R. R.; Misra, M. *Int. J. Hydrogen Energy* **2009**, *34*, 3250−3257.
(12) Roy, P.; Kim, D.; Lee, K.; Spiecker, E.; Schmuki, P. *Nanoscale* **2010**, *2*, 45−59.
(13) Sharmoukh, W.; Allam, N. K. *ACS Appl. Mater. Interfaces* **2012**, *4*, 4413−4418.
(14) Ghicov, A.; Tsuchiya, H.; Hahn, R.; Macak, J. M.; Muñoz, A. G.; Schmuki, P. *Electrochem. Commun.* **2006**, *8*, 528−532.
(15) Berger, S.; Ghicov, A.; Nah, Y.-C.; Schmuki, P. *Langmuir* **2009**, *25*, 4841−4844.
(16) Gandhi, T.; Raja, K. S.; Misra, M. *Electrochim. Acta* **2006**, *51*, 5932−5942.
(17) Liu, S.; Chen, A. *Langmuir* **2005**, *21*, 8409−8413.
(18) Kar, A.; Raja, K. S.; Misra, M. *Surf. Coat. Technol.* **2006**, *201*, 3723−3731.
(19) Oh, S.; Daraio, C.; Chen, L.-H.; Pisanic, T. R.; Fiñones, R. R.; Jin, S. *J. Biomed. Mater. Res. A* **2006**, *78A*, 97−103.
(20) Chen, B.; Lu, K. *Langmuir* **2011**, *27*, 12179−12185.
(21) Kar, A.; Smith, Y. R.; Subramanian, V. R. *Environ. Sci. Technol.* **2009**, *43*, 3260−3265.
(22) Liu, Z.; Misra, M. *ACS Nano* **2010**, *4*, 2196−2200.
(23) Liu, Z.; Subramanian, V.; Misra, M. *J. Phys. Chem. C* **2009**, *113*, 14028−14033.
(24) Smith, Y. R.; Subramanain, V. *J. Phys. Chem. C* **2011**, *115*, 8376−8385.
(25) Liao, J.; Lin, S.; Zhang, L.; Pan, N.; Cao, X.; Li, J. *ACS Appl. Mater. Interfaces* **2012**, *4*, 171−177.

(26) Chappanda, K. N.; Smith, Y. R.; Misra, M.; Mohanty, S. K. *Nanotechnology* **2012**, *23*, 385601.
(27) Chappanda, K. N.; Smith, Y. R.; Mohanty, S. K.; Rieth, L. W.; Tathireddy, P.; Misra, M. *Nanoscale Res. Lett.* **2012**, *7*, 388.
(28) Roy, P.; Berger, S.; Schmuki, P. *Angew. Chem., Int. Ed.* **2011**, *50*, 2904−2939.
(29) Misra, M.; Raja, K. S. In *On Solar Hydrogen & Nanotechnology*; Vayssieres, L., Ed.; John Wiley & Sons: Chichester, U.K., 2010; Vol. *1*, pp 266−290.
(30) Park, J. H.; Kim, S.; Bard, A. J. *Nano Lett.* **2006**, *6*, 24−28.
(31) Ghicov, A.; Macak, J. M.; Tsuchiya, H.; Kunze, J.; Haeublein, V.; Frey, L.; Schmuki, P. *Nano Lett.* **2006**, *6*, 1080−1082.
(32) Sohn, Y. S.; Smith, Y. R.; Raja, K. S.; Subramanian, V.; Misra, M. In *Solar Hydrogen and Nanotechnology II*; Guo, J., Ed.; SPIE: San Diego, CA, 2007; Vol. *6650*, pp K1−K11.
(33) Banerjee, S.; Mohapatra, S. K.; Das, P. P.; Misra, M. *Chem. Mater.* **2008**, *20*, 6784−6791.
(34) Banerjee, S.; Mohapatra, S. K.; Misra, M. *J. Phys. Chem. C* **2011**, *115*, 12643−12649.
(35) Mukherjee, B.; Smith, Y. R.; Subramanian, V. R. *J. Phys. Chem. C* **2012**, *116*, 15175−15184.
(36) Sharma, R.; Das, P. P.; Misra, M.; Mahajan, V.; Bock, J. P.; Trigwell, S.; Biris, A. S.; Mazumder, M. K. *Nanotechnology* **2009**, *20*, 075704.
(37) Murugesan, S.; Smith, Y. R.; Subramanian, V. *J. Phys. Chem. Lett.* **2010**, *1*, 1631−1636.
(38) Smith, Y. R.; Sarma, B.; Mohanty, S. K.; Misra, M. *Electrochem. Commun.* **2012**, *19*, 131−134.
(39) Harris, L. A.; Wilson, R. H. *J. Electrochem. Soc.* **1976**, *123*, 1010−1015.
(40) Sugiura, T.; Yoshida, T.; Minoura, H. *Electrochem. Solid St.* **1998**, *1*, 175−177.
(41) Nakato, Y.; Akanuma, H.; Shimizu, J.-i.; Magari, Y. *J. Electroanal. Chem.* **1995**, *396*, 35−39.
(42) Smith, R. L.; Collins, S. D. *J. Appl. Phys.* **1992**, *71*, R1.
(43) Sohn, Y. S.; Smith, Y. R.; Subramanian, V. R.; Misra, M. *Appl. Catal. B: Environ.* **2008**, *84*, 372−378.
(44) Mohapatra, S. K.; Raja, K. S.; Misra, M.; Mahajan, V. K.; Ahmadian, M. *Electrochim. Acta* **2007**, *53*, 590−597.
(45) Zhang, L.; Koka, R. V. *Mater. Chem. Phys.* **1998**, *57*, 23−32.
(46) Sakthivel, S.; Kisch, H. *Angew. Chem., Int. Ed.* **2003**, *42*, 4908−4911.
(47) Chen, D.; Jiang, Z.; Geng, J.; Wang, Q.; Yang, D. *Ind. Eng. Chem. Res.* **2007**, *46*, 2741−2746.
(48) Raja, K. S.; Mahajan, V. K.; Misra, M. *J. Power. Sources.* **2006**, *159*, 1258−1265.
(49) Raja, K. S.; Misra, M.; Mahajan, V. K.; Gandhi, T.; Pillai, P.; Mohapatra, S. K. *J. Power Sources* **2006**, *161*, 1450−1457.
(50) Wu, Z.; Dong, F.; Zhao, W.; Wang, H.; Liu, Y.; Guan, B. *Nanotechnology* **2009**, *20*, 235701.
(51) Breckenridge, R. G.; Hosler, W. R. *Phys. Rev.* **1953**, *91*, 793−802.
(52) Subramanian, V. *Interface* **2007**, *16*, 32−36.
(53) Zhang, Z.; Yu, Y.; Wang, P. *ACS Appl. Mater. Interfaces* **2012**, *4*, 990−996.
(54) Bard, A. J.; Faulkner, L. R. *Electrochemical Methods: Fundamentals and Applications*, 2nd ed.; John Wiley & Sons: New Delhi, 2004; Vol. *1*, p 751−754.
(55) Raja, K. S.; Smith, Y. R.; Kondamudi, N.; Manivannan, A.; Misra, M.; Subramanian, V. *Electrochem. Solid St.* **2011**, *14*, F5−F8.
(56) Dittrich, T.; Lebedev, E. A.; Weidmann, J. *Phys. Status Solidi A.* **1998**, *165*, R5.
(57) Sukamto, J. P. H.; Mcmillan, C. S.; Smyrl, W. *Electrochim. Acta* **1993**, *38*, 15−27.
(58) Macak, J. M.; Tsuchiya, H.; Schmuki, P. *Angew. Chem., Int. Ed.* **2005**, *44*, 2100−2102.
(59) Vrublevsky, I.; Parkoun, V.; Schreckenbachb, J.; Marx, G. *Appl. Surf. Sci.* **2003**, *220*, 51−59.
(60) Song, Y.-Y.; Schmuki, P. *Electrochem. Commun.* **2010**, *12*, 579−582.
(61) Albu, S. P.; Kim, D.; Schmuki, P. *Angew. Chem., Int. Ed.* **2008**, *47*, 1916−1919.